Journal of Materials Chemistry A

Accepted Manuscript

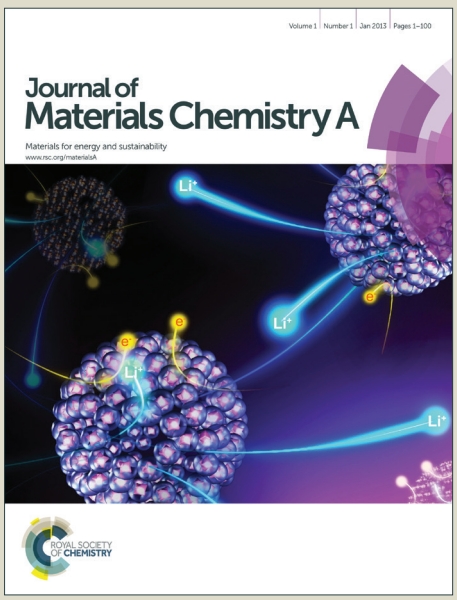

This is an *Accepted Manuscript*, which has been through the Royal Society of Chemistry peer review process and has been accepted for publication.

Accepted Manuscripts are published online shortly after acceptance, before technical editing, formatting and proof reading. Using this free service, authors can make their results available to the community, in citable form, before we publish the edited article. We will replace this *Accepted Manuscript* with the edited and formatted *Advance Article* as soon as it is available.

You can find more information about *Accepted Manuscripts* in the Information for Authors.

Please note that technical editing may introduce minor changes to the text and/or graphics, which may alter content. The journal's standard Terms & Conditions and the Ethical guidelines still apply. In no event shall the Royal Society of Chemistry be held responsible for any errors or omissions in this *Accepted Manuscript* or any consequences arising from the use of any information it contains.

ROYAL SOCIETY OF CHEMISTRY

www.rsc.org/materialsA

Design of mesoporous silica hybrid materials as sorbents for the selective recovery of rare earth metals

Xudong Zheng, Chun Wang, Jiangdong Dai, Weidong Shi, Yongsheng Yan*

School of Chemistry & Chemical Engineering, Jiangsu University, Zhenjiang 212013, PR China

Abstract:

The importance of rare earth metals in the global economy has increased significantly in recent years due to their essential role in advanced technologies in the electronics and biomedical industries. The recovery and purification of rare earths metals from waste products is therefore appealing, both in terms of the sustainability of rare earth resources and ecological environmental protection. We herein present the preparation of novel mesoporous silica materials modified by maleic anhydride, which can be used in the recovery of rare earth metals through extraction of their ions from an aqueous solution. Our novel maleic anhydride functional hybrid materials demonstrate enhanced selectivity for heavy rare earth metals, which vastly improves the separation process and reduces recovery costs. In addition, the directly modified hybrid materials have been found to exhibit higher distribution coefficients for rare earth elements compared to other materials. Adsorption kinetics studies were also carried out, and the adsorption followed a pseudo-second order model, with particularly rapid adsorption observed in the case of Gd^{3+}. The resulting adsorption isotherms of the materials were better represented by the Langmuir model than the Freundlich model. The singly modified material exhibited a Gd^{3+} capture capacity of 76.89 mg g^{-1}. In addition, the proposed materials demonstrate a high degree of reusability over a number of cycles, thus enhancing their potential for application in rare earth metal recycling.

Journal of Materials Chemistry A Accepted Manuscript

1. Introduction

The rare earth metals (REMs) are a group of elements consisting of the 15 lanthanides plus scandium and yttrium. They are found in numerous products, ranging from cars to smart phones and green energy products. Over the last few decades, the global consumption rate of REMs has increased significantly because of their use in catalysis,[1, 2] chemical sensors,[3] optical materials,[4-9] and various chemical engineering applications.[10-15] However, stricter management and export restraints from China (who produce approximately 90% of the global REM output) have clearly exacerbated the worldwide REM supply shortage. In addition, pollution from the mining of raw materials and from the production of REM waste is having a serious impact on the sustainability, utilisation, and environmental impact of REM resources. To solve these issues, an effective absorbent material must be developed urgently for the recovery and enrichment of REMs, especially from waste sources.

However, despite these serious issues, industrial recycling of REMs remains at critically low levels. Separation and pre-enrichment of the individual rare earth elements is extremely complex, as they possess only subtle differences in their chemical properties.[16] Efforts for the efficient recovery of REMs are underway, but progress remains slow.[17, 18] The frontrunner in these investigations, Chalmers University of Technology, have studied the recovery of REMs from fluorescent lamp waste, focusing specifically on cerium (Ce), europium (Eu), gadolinium (Gd), lanthanum (La), terbium (Tb), and yttrium (Y).[19] They also investigated the effects of a range of parameters for their recovery, including a number of leaching solutions, variation in temperature, different solid/liquid ratios, and various sorbent concentrations. A range of optimisation experiments suggested that solvent extraction was likely to be a viable method for the recovery of REMs. However, depending on the values of individual rare earth metals in industrial applications, it may not be desirable to recover all REMs for recycling. As acknowledged by the U.S. Department of Energy (DOE), the five most important REMs for recovery are neodymium (Nd), europium (Eu), terbium (Tb), dysprosium (Dy), and yttrium (Y).[20]

Journal of Materials Chemistry A Accepted Manuscript

In addition, the recovery of gadolinium (Gd) has increased in importance because of its unique magnetic and optical characteristics. As the majority of rare earth elements in imperative demand are the heavy REMs, the separation of these elements is of enormous value in industry.

Recently, extraction chromatographic resins (EXC) have been applied for use in the preferential adsorption of REMs.[21-23] Among the EXCs, mesoporous materials were found to exhibit high surface areas, allowing for greatly enhanced adsorption capacities, and were indeed proven to be promising for adsorption applications in the selective capture and removal of heavy metals.[24, 25] In addition, mesoporous silica materials present an abundant number of silanol groups on their surfaces, allowing for functionalization by chemical grafting.[26-28] Indeed, mesoporous silica nanoparticles have attracted a great amount of attention for their potential application in the fields of biomedicine,[29, 30] heterogeneous catalysis,[31] and separation.[32] Furthermore, the pore size, pore shape, and dimensions of the mesoporous silica nanoparticles can be designed to optimise adsorption and separation performance in the extraction processes. Due to the presence of the silanol groups on the mesoporous surfaces, the possibility exists to chemically anchor extracting agents (ligand modified) to enhance the REM adsorption selectivity. Solid phase extraction (SPE) is a simple and green extraction technique compared to the multiple liquid-liquid extraction strategies for the separation and purification of heavy REMs which currently exist. Such liquid-liquid extraction techniques require a large volume of organic solvent over continuous, repeated steps, which are not only time-consuming, but also produce a large quantity of undesired waste. Justyna and co-workers therefore developed a feasible process to recycle REMs from mining residues using a solid-liquid system,[33] employing a diglycolylamide-modified mesoporous silica as a candidate for REM separation. This modified material also displayed a much higher affinity for the separation of the heavy lanthanides, and so this method has great potential for its application prospects. However, the design of a selective REM ligand is still required, particularly for REMs such as Eu and Gd.

We therefore propose the use of a mesoporous silica support modified by maleic

Journal of Materials Chemistry A Accepted Manuscript

anhydride (MAH) with the aim of developing a selective recovery system for REMs. Maleic anhydride is a commonly used organic anhydride which is produced industrially on a large scale for use in coatings and polymers. In the strategy reported here, MAH was chemically grafted to the surface of the silica support, with the aim of improving the regeneration stability of the silica materials, and increasing the selectivity to heavy REM extraction (especially Gd^{3+}). REMs adsorption was studied using a solid-liquid system, where the distribution coefficients (K_d), adsorption kinetics, and adsorption isotherm data were used to determine the adsorption properties and selectivities of the materials under the test conditions. Moreover, the use of relatively cheap ligands, and the reusability of the extraction materials renders this process particularly cost-effective and economically viable while minimising pollution and improving environmental sustainability.

2. Experimental

2.1 Preparation of materials

All reagents used were analytical standard. And double distilled water was used throughout the experimental procedures.

Synthesis of mesoporous silica nanoparticles (MSNP): The unmodified MSNP-OH particles were synthesised according to previously reported literature methods.[34, 35] Cetyltrimethylammonium bromide (CTAB, 500 mg) was dissolved in a solution of water (240 mL) and sodium hydroxide (1.75 mL, 2.0 M) and heated to 80 °C with stirring. Tetraethyl orthosilicate (TEOS, 2.5 mL) was then added dropwise to the surfactant solution. The mixture was allowed to stir vigorously at 80 °C for 2 h. After this time, the resulting solid was filtered, and dried overnight at 100 °C. The CTAB surfactants were subsequently removed by calcination at 550 °C over 6 h, to give the desired product (MSNP-OH).

Two step surface modification of MSNP-OH: Activated MSNP-OH (1.0 g) was dispersed in dry toluene (75 mL) under N_2. (3-Aminopropyl) triethoxysilane (APTES, 2.0 mL) was added to the dispersion, and then stirred for 24 h under reflux. The

Journal of Materials Chemistry A Accepted Manuscript

resulting product was filtered, washed with toluene and ethanol three times, and dried overnight in air at 60 °C. The resulting material (MSNP-N) was then subjected to functionalization as follows. MSNP-N (0.25 g) was dispersed in *N,N'*-dimethylformamide (DMF, 15 mL) under N_2, and MAH (0.35 g) and pyridine (0.25 mL) added to the dispersion. The resulting mixture was allowed to stir for 3 h at 50 °C. During the reaction, the colour of the mixture changed from colourless to bronze. The suspended product was then filtered, washed with toluene and ethanol three times, and dried overnight at 60 °C to give the desired product, MSNP-N-1.

Direct functionalization of MSNP-OH: MAH (0.05 mol, 5.0 g) and water (10 mL) were added to a 100 mL round bottom flask and allowed to stir overnight under N_2 to give hydrolysis of the MAH. The generated MAc was filtered, washed with $CHCl_3$ three times, and dried in a vacuum oven.

MAc (4.0 g) was then added to a round bottom flask, which was placed in an ice/water bath under N_2. $SOCl_2$ (5.0 mL) was added dropwise to the MAc over 6 h with stirring. After this time, excess $SOCl_2$ was removed at reduced pressure. The resulting product was dissolved in $CHCl_3$, filtered, and solvents removed at reduced pressure. The crude maleic acid chloride (MACl) was used in the following step without further purification. δH (400 MHz, $CDCl_3$) 7.03 (2H, s).

APTES (2.0 mL) was dissolved in dry toluene (20 mL) under N_2. MACl (4.0 mmol) was then added to dry toluene (30 mL) and the resulting mixture added to the APTES solution. Triethylamine (TEA, 1.2 mL) was used as catalyst. The mixture was allowed to stir under reflux for 12 h under a flow of N_2, and the modified silane used directly without further purification. Activated MSNP-OH (1.0 g, treated overnight at 150 °C) was dispersed in dry toluene (50 mL), and the above modified silane solution added rapidly to the suspension. The resulting mixture was stirred for 24 h under reflux. After cooling to room temperature, the suspended solid product was filtered, washed with toluene and ethanol three times, and dried overnight at 60 °C in air to give the desired product, MSNP-N-2.

The synthetic approach for the modified materials is depicted in Scheme 1.

Journal of Materials Chemistry A Accepted Manuscript

2.2 Characterisation of materials

FTIR spectra (4000-400 cm^{-1}) were collected on a Nicolet NEXUS-470 FT-IR apparatus (U.S.A.) using KBr disks. Transmission electron microscopy (TEM) was performed using a JEOL JEM-2100 (HR) at an accelerating voltage of 200 kV with a LaB6 filament. Low angle powder X-ray diffraction (XRD) measurements were made using a D8 ADVANCE diffractometer (Germany Bruker). Elemental analysis was performed using the combustion method on a CHNS Analyzer Flash 1112A (Thermo Scientific). The size distribution of the particles was measured at 25 ℃ using dynamic light scattering (DLS) with high laser concentrations, using a particle size analyzer (BI-9000, Brookhaven, NY). All the samples were suspended in water at a concentration of 100 μg mL^{-1}, and filtered through Supor filters (0.45 μm) to remove any possible dust. The DLS size distribution was plotted using a log-normal analysis method. ^{1}H nuclear magnetic resonance (NMR) was carried out on a 400 MHz Bruker AVANCE Ⅱ. Proton chemical shifts (δ) are reported as shifts from the internal standard tetramethylsilane (TMS). Thermogravimetric analysis (TGA) was measured using a Diamond TG/DTA Instruments (STA 449C Jupiter, Netzsch, Germany) under a nitrogen atmosphere up to 600 °C with a heating rate of 10 °C min^{-1}. The surface area was determined using N_2 adsorption isotherms on the sorbent using a Micromeritics TriStar II 3020 analyzer (Micromeritics Instrument Corporation, USA). All materials (pristine and modified materials) were dried under reduced pressure at 50 °C for 12 h and were outgassed for either 6 h at 100 °C (parent silica), or 6 h at 60 °C (functionalised sorbents) prior to N_2 adsorption analysis, which was carried out at -196 °C. The surface area was obtained by a multi-point analysis of the volume of nitrogen adsorbed as a function of relative pressure.

2.3 Adsorption experiments

Static adsorption tests: Stock solutions of a range of elements (Sm, Eu, Gd, Tb, Dy, Ho, Er, Al, and Fe) in HNO_3 (pH=4) were prepared from the standards solutions, in

Journal of Materials Chemistry A Accepted Manuscript

order to obtain a final concentration of 20 mg L^{-1} for each element. Samples (10 mg) of the four nanomaterials (MSNP-OH, MSNP-N, MSNP-N-1, and MSNP-N-2) were added to portions of the stock solutions (10 mL) and were stirred in an orbital shaker for 4 h. The supernatant was then filtered through Supor filters (0.22 μm), and the initial and final concentrations of the REM solutions were determined by ICP-OES (ICP spectrometer, VARIAN America). This process was repeated in triplicate.

Adsorption kinetics: Samples (10 mg) of the four nanomaterials (MSNP-OH, MSNP-N, MSNP-N-1, and MSNP-N-2) were added to the Gd^{3+} stock solution (10 mL, 50 mg L^{-1}, pH = 4) and stirred in an orbital shaker. The samples were then filtered through Supor filters (0.22 μm). The residual Gd^{3+} concentrations were detected by ICP-OES. This process was repeated in triplicate

Adsorption isotherms: Samples (10 mg) of the four nanomaterials (MSNP-OH, MSNP-N, MSNP-N-1, and MSNP-N-2) were added to the Gd^{3+} stock solutions (10 mL, pH = 4), and stirred in an orbital shaker for 4 h to reach equilibrium. The samples were then filtered through Supor filters (0.22 μm). The residual Gd^{3+} concentrations were detected by ICP-OES. This process was repeated in triplicate

2.4 Reusability tests

Following the adsorption tests, the MSNP-N-2 (10 mg) was separated from the residue solution by centrifugation. The fractions containing unretained rare earth elements (REE) were examined by ICP-OES. The sorbents were then rinsed with acetonitrile (2 mL) and double distilled water (10 mL). The material was regenerated using 4% HNO_3, and the reconditioned MSNP-N-2 used in sequential experiments, repeating the adsorption procedure to achieve 5 cycles.

3. Results and discussion

3.1 Characterisation of the materials

The synthesis of MSNP was carried out according to a modified sol-gel procedure.

Journal of Materials Chemistry A Accepted Manuscript

Subsequent functionalization of MSNP with ligands was performed in dry toluene under a nitrogen atmosphere. The resulting surface-modified MSNPs were assigned the following codes: MSNP-OH, MSNP-N, MSNP-N-1, MSNP-N-2, denoting before (OH) and after (N) APTES treatment, using either a one- (2) or two-step (1) sequence.

3.1.1 Structural characterisation

The 2-dimensional mesoporous structure of the modified materials was verified by transmission electron microscopy (TEM), and low angle powder X-ray diffraction (XRD). Examination of the TEM images showed that the size of the MSNP-OH was approximately 80-120 nm, and it possessed pores of uniform size (approx. 2 nm, Figures 1a and 1b). Treatment of MSNP-OH with APTES to give MSNP-N resulted in changes to the mesoporous structure and surface roughness due to the silicone modification, as can be seen in Figures 1c and 1d. In addition, the TEM images of MSNP-N-1 (Figures 1e and 1f) showed no significant difference in structure compared to MSNP-N, whereas that of MSNP-N-2 displayed an ordered mesoporous structure as in the case of MSNP-OH. This confirms that although the directly functionalised materials were subjected to the grafting sequence, the ordered pore structure remained intact, and similar to that of the parent silica. XRD patterns of pure samples of MSNP-OH, MSNP-N, MSNP-N-1, and MSNP-N-2 are shown in Figure 1i. The mesostructure of the materials was revealed to be comparable with previously reported results.[36] The hydrodynamic diameters of the four materials were measured using dynamic light scattering (DLS) (Figure S1), and were found to be 119.3, 130.4, 132.1, and 123.9 nm for MSNP-OH, MSNP-N, MSNP-N-1, and MSNP-N-2, respectively. These values are substantially larger than those estimated from the TEM images, which may be due to the presence of oblate ellipsoidal nanoparticles in the resulting materials.

The corresponding values for the specific surface areas and pore size distributions (PSD) for the original and functionalised MSNPs are shown in Figure 2. Typical type IV isotherms with distinctive H1 hysteresis loops were observed for all materials,

Journal of Materials Chemistry A Accepted Manuscript

which were found to exhibit characteristics comparable with cylindrical mesopores.[37] The Brunauer-Emmett-Teller (BET) surface area of the pristine MSNP-OH was calculated as approximately 575 $m^2 g^{-1}$. Surface modification by the grafting of MA to the silica support resulted in a decrease in pore size, leading to the capillary condensation step shifting to lower values of relative pressure (P/P_o). Analogous evolution was observed for the surface area and pore volume of MSNP-N-1 which displayed the lowest values of all the materials.

3.1.2 Surface characterisation

To confirm the covalent attachment of the organic species on the MSNP-OH surface, Fourier transform infrared spectra (FT-IR), thermogravimetric analysis, and elemental analysis were performed.

The infrared spectra of MSNP-OH, MSNP-N, MSNP-N-1, and MSNP-N-2 are shown in Figure 3. The adsorption peaks at 1091 cm^{-1} and 3432 cm^{-1} in the spectra of all silica spheres could be assigned to the Si-O-Si asymmetric stretching vibration and the Si-OH stretching vibration, respectively. In addition, signals at 1650 cm^{-1} and 1550 cm^{-1} in the spectra of MSNP-N-1 and MSNP-N-2 were assigned to the CO stretching vibration (Amide I) and NH deformation vibration (Amide II), respectively, thus confirming the presence of amide bonds in the modified hybrid solids. In addition, the presence of a second signal corresponding to a CO stretching vibration was observed in the spectra of MSNP-N-1 due to the range of grafted patterns present (Scheme 1). From the FT-IR results, it could therefore be concluded that surface modification was successfully achieved on the silica support.

The degree of functionalization of the four materials was evaluated by thermogravimetric analysis under a nitrogen atmosphere. Modified materials MSNP-N-1 and MSNP-N-2 gave a total weight loss of approximately 28.84% and 30.87%, respectively, compared to 25.04% loss for MSNP-N (Figure 4), and 13.48% for the pure silica material. With the initial temperature range (<150 °C), the weight losses were attributed largely to the loss of residual water, confirming the expected hydrophilicity of the materials. This hydrophilicity is beneficial for the recovery of

Journal of Materials Chemistry A Accepted Manuscript

REMs in water, and so is particularly important in the context of our study. Thermal decomposition of the functionalised sorbents was found to occur between 175 and 700 °C, with significant weight losses in the case of MSNP-N-1 and MSNP-N-2 being assigned to the decomposition of MA. CHN elemental analysis was also carried out to determine the quantities of carbon, nitrogen, and hydrogen in the modified samples. The results of these analyses are given in Table 1. The carbon and nitrogen compositions of MSNP-N were found to increase to 14.39% and 4.962%, with respect to MSNP-OH. In the case of the two modified samples, the carbon and nitrogen contents were comparable. In addition, Mohr's method was carried out to determine the chloride contents of both MSNP-N-1 and MSNP-N-2 (Table 1). Low levels of chloride ions in MSNP-N-1 confirmed successful substitution of the chlorine atoms in MACl.

3.2 Adsorption studies

3.2.1 Static adsorption studies

Adsorption experiments for the REMs of interest (Sm, Eu, Gd, Tb, Dy, Ho, and Er) and additional ions (Al and Fe) were performed on MAH-modified MSNP and bulk MSNP materials. In addition, the sorption performances of modified MSNP materials with respect to the REMs were evaluated in terms of the distribution coefficients (K_d, mL g^{-1}) which were calculated according to Equation 1:

$$k_d = \frac{C_o - C}{C} \times \frac{V}{m} \quad (1)$$

where, C_o and C are the initial and final concentration of the REM, respectively, and V and m are the volume of solution and sorbent mass used, respectively.

From the results of the adsorption tests, it was clear that MAH-modification of MSNPs enhanced the value of K_d compared to the unmodified MSNP-OH or MSNP-N (Figure 5), with higher K_d values representing more effective sorbents for

Journal of Materials Chemistry A Accepted Manuscript

the separation of REMs.[38] Based on the structures of the materials examined herein, we expect that the high K_d value can attributed to the ligand chelation mechanism. According to the HSAB theory (hard and soft acids and bases theory), the two carbonyl groups of the MA ligand belong to the group of hard bases, which have excellent selectivity for the coordination of Ln^{3+} (typical hard acids) over other competing trivalent ions of environmental and mining relevance (*e.g.* Al^{3+} and Fe^{3+}). One may hypothesise that the highly selective adsorption towards REMs could be due to a synergy of steric effects and electrostatic interactions that may be more noticeable on a solid support than in the liquid phase. The means that the rigid structure of the silicon matrix could therefore offer an excellent spatial structure for the coordination of Ln^{3+} with the two carbonyl oxygen atoms of the organic ligand. Furthermore, the rigid silica structure prevents the ligands forming more stable chelate rings, thus favouring the chelation of REMs to ions of a certain radius. In addition, in contrast to MSNP-N-1, more pronounced selectivity was observed for MSNP-N-2, which displayed a particularly high adsorption capacity for Gd^{3+} (K_d = 2673 mL g^{-1}). This difference may arise from the presence of residual -NH_2 groups on the surface of MSNP-N-1 (prepared in two steps), which are absent in the material prepared *via* the one step procedure. As the -NH_2 groups exhibit Lewis basic characteristics, this decreases their selectivity towards the REMs. It is also possible that chelating rings of ligand and the presence of a micro-environment on the surface, resulted in size specific selectivity towards Ln^{3+} of a certain radius.

3.2.2. Adsorption kinetics

The adsorption behaviour of the sorbents towards the REMs was then investigated. In order to determine the rate-controlling mechanism of the adsorption process, adsorption kinetic experiments were conducted. The sorbent materials were dispersed in stock solutions of Gd^{3+} and the residual Gd^{3+} detected after a defined range of adsorption times. The amount of REM adsorbed at time *t* was calculated using the following relationship:

Journal of Materials Chemistry A Accepted Manuscript

$$Q_t = \frac{(C_0 - C_t)V}{W} \quad (2)$$

where Q_t (mg g^{-1}) is the amount of Gd^{3+} absorbed, C_0 (mg L^{-1}) and C_t (mg L^{-1}) are the initial and final Gd^{3+} concentrations in solution before and after time t, V and W are the solution volume (L) and sorbent mass (g) used in the tests, respectively.

The kinetic data of MSNP-OH, MSNP-N, MSNP-N-1, and MSNP-N-2 shown in Figure 6 were analysed by pseudo-first-order and pseudo-second-order kinetic models as given below:

$$Q_t = Q_e - Q_e e^{-k_1 t} \quad (3)$$

$$Q_t = \frac{k_2 Q_e^{\,2} t}{1 + k_2 Q_e t} \quad (4)$$

where Q_t (mg g^{-1}) and Q_e (mg g^{-1}) are the amount of Gd^{3+} adsorbed at time t, and at equilibrium, respectively. k_1 (L min^{-1}) and k_2 (g mg^{-1} min^{-1}) are the rate constants of the pseudo-first-order and pseudo-second-order models. The results for these analyses are given in Table 2. Based on the pseudo-second-order kinetic rate constant, the initial adsorption rate h (mg g^{-1} min^{-1}) and half equilibrium time $t_{1/2}$ (min) can also be incorporated, according to the following equations (see also Table 2):[39]

$$h = k_2 Q_e^{\,2} \quad (5)$$

$$t_{1/2} = \frac{1}{k_2 Q_e} \quad (6)$$

As shown in Figure 6, the kinetic curves of these four materials increased rapidly, particularly in the first 60 min, finally reaching equilibrium within 2-4 h. MSNP-N-2 was found to display a significantly higher adsorption equilibrium capacity than the other materials, implying greater specificity of MSNP-N-2 towards the REMs. In

Journal of Materials Chemistry A Accepted Manuscript

terms of adsorption kinetics models, the pseudo-second-order model appeared to be a better fit for the adsorption of REMs by both MSNP-N-1 and NSNP-N-2, with correlation coefficients of 0.987 and 0.985, respectively. Moreover, the calculated Q_e values of the pseudo-second-order equation were also closer to the experimental Q_e data than those of the pseudo-first-order kinetic model. These results suggested that the chemical process was likely to be the rate-limiting step of the adsorption mechanism. At equal time, the h and $t_{1/2}$ data for MSNP-N-1 and MSNP-N-2 were found to be significantly better than for MSNP-OH and MSNP-N (Table 2), indicating that the presence of organic moieties improves the kinetic properties of the materials. In addition, MSNP-N-2 was found to display superior kinetic properties compared to MSNP-N-1.

3.2.3. Adsorption isotherms

Adsorption equilibrium curves were established to analyse and compare the adsorption performance properties of the four sorbents, including the nonlinear dynamic balance of the solution and the solute between the different materials. Adsorption isotherms were determined using a series of Gd^{3+} stock solutions of varying concentration. The sorbent materials were dispersed in each stock solution and shaken for 4 h to achieve equilibrium. The binding properties of the materials with respect to Gd^{3+} were evaluated by equilibrium adsorption experiments at 25 °C as shown in Figure 7, along with the absorption equilibrium data fit to the Langmuir[40] and Freundlich[41] isotherm models. The nonlinear equations of the two isotherm models are expressed as follows:

$$Q_e = \frac{K_L Q_m C_e}{1 + K_L C_e} \quad (7)$$

$$Q_e = K_F C_e^{1/n} \quad (8)$$

Journal of Materials Chemistry A Accepted Manuscript

where C_e (mg L^{-1}) represents the adsorption equilibrium concentration in solution, Q_e (mg g^{-1}) is the equilibrium adsorption capacity, Q_m (mg g^{-1}) represents the maximum adsorption capacity of the materials, K_L (L g^{-1}) is the affinity constant, K_F (mg g^{-1}) is the sorbent adsorption capacity direction constant, and 1/n indicates favourable adsorption conditions.

It was found that the adsorption capacity of MSNP-N-2 was higher than that of MSNP-N-1 under the same conditions, suggesting a preference of MSNP-N-2 for Gd^{3+}. In addition, the Langmuir isotherm model gave a better fit to the experimental adsorption data (R^2>0.94, Table 3), indicating a uniform solid surface on the sorbents, and a regular monolayer, resulting in finite molecular adsorption. From the experimental data of MSNP-N-1 and MSNP-N-2, we observed that the adsorption capacity increased with an increase in Gd^{3+} content. The experimental saturation capacities for MSNP-N-1 and MSNP-N-2 were found to be 46.94 mg g^{-1} and 76.89 mg g^{-1}, which are comparable to the equilibrium sorption capacities (Q_m) calculated using the Langmuir model (56.22 mg g^{-1} and 85.38 mg g^{-1}). In addition, based on the Langmuir model, the favourability of sorbent, related to the separation factor R_L, can be obtained using the value of K_L (Equation 9), where C_m is the maximum initial metal ion concentration:

$$R_L = \frac{1}{1 + C_m K_L} \quad (9)$$

According to equation 9, a value of $0 < R_L < 1$ indicates that the sorbent is a favourable medium for the adsorption of the given metal ion. The obtained values of R_L for MSNP-N-1 and MSNP-N-2 were calculated to be 0.0929 and 0.0463, respectively, thus confirming that MSNP-N-2 is a more favourable sorbent for Gd^{3+}.

3.3. Reusability tests

Acceptable regeneration performance is a key factor when considering the use and

Journal of Materials Chemistry A Accepted Manuscript

value of such sorbent materials. Recyclability tests were therefore carried out to evaluate the regeneration ability of MSNP-N-2 in terms of REM recovery, using a mixture of REMs (Sm, Eu, Gd, Tb, Dy, Ho, and Er). The results for five adsorption/regeneration cycles are shown in Figure 8. As can be seen from Figure 8, the adsorption ability of MSNP-N-2 towards REMs reduced to approximately 93.15% of the value of the first cycle, likely due to a reduction in binding ligand sites following regeneration. Finally, the stability of the organic groups was confirmed by TGA (Figure S5), with no distinct changes in the sorbent material being observed after 5 cycles. This suggests that MSNP-N-2 has excellent chemical stability as a highly efficient adsorbent for the recovery of REMs.

4. Conclusions

In summary, novel low-cost sorbents composed of maleic anhydride functional mesoporous silica were prepared by controlled ligand grafting to the silica support, and were applied in the adsorption of lanthanides. The sorbent materials exhibited selective bonding to the REMs, and in particular to Eu^{3+} and Gd^{3+}, likely related to the suitable geometries derived from their preparation. The material prepared *via* a one-step method, namely MSNP-N-2, displayed significantly higher adsorption performances than the other resins. The sorption of Gd^{3+} was found to follow pseudo-second-order type sorption kinetics. Overall, it was observed that the initial kinetics of REM sorption were fast, with almost complete adsorption observed after 100 min. In addition, the sorption isotherms for Gd^{3+} were successfully modelled using the Langmuir isotherm, which revealed a monolayer adsorption mechanism. In conclusion, as the efficient recycling of REMs requires the development of environmentally-friendly and low-cost recycling materials, we have demonstrated that the MAH-modified materials presented herein have great potential for practical routine application in REM recovery.

Journal of Materials Chemistry A Accepted Manuscript

Acknowledgements

This work was financially supported by the National Natural Science Foundation of China (No. 21176107, No. 21107037, No. 21277063, No. 21346004), the Specialized Research Fund for the Doctoral Program of Higher Education of China (20133227110010), and the Natural Science Foundation of Jiangsu Province (No. BK20140534, No. BK20140535).

Notes and references

1. J. Christoffers, T. Werner and M. Roessle, *Catal. Today*, 2007, **121**, 22-26.
2. M. Rössle and J. Christoffers, *Tetrahedron*, 2009, **65**, 10941-10944.
3. X. Zheng, J. Pan, L. Gao, X. Wei, J. Dai, W. Shi and Y. Yan, *Microchim. Acta*, 2014, **182**, 753-761.
4. N. Venkatachalam, T. Yamano, E. Hemmer, H. Hyodo, H. Kishimoto and K. Soga, *J. Am. Ceram. Soc.*, 2013, **96**, 2759-2765.
5. J. Massue, S. J. Quinn and T. Gunnlaugsson, *J. Am. Chem. Soc.*, 2008, **130**, 6900-6901.
6. Q. Ju, D. Tu, Y. Liu, R. Li, H. Zhu, J. Chen, Z. Chen, M. Huang and X. Chen, *J. Am. Chem. Soc.*, 2011, **134**, 1323-1330.
7. N. Davydov, R. Zairov, A. Mustafina, V. Syakayev, D. Tatarinov, V. Mironov, S. Eremin, A. Konovalov and M. Mustafin, *Anal. Chim. Acta*, 2013, **784**, 65-71.
8. M. Kaljurand, *Trends in Environmental Analytical Chemistry*, 2014, **1**, e2-e7.
9. S. R. Subashchandrabose, K. Krishnan, E. Gratton, M. Megharaj and R. Naidu, *Environ. Sci. Technol.*, 2014, **48**, 9152-9160.
10. I. V. Melnyk, V. P. Goncharyk, L. I. Kozhara, G. R. Yurchenko, A. K. Matkovsky, Y. L. Zub and B. Alonso, *Microporous Mesoporous Mater.*, 2012, **153**, 171-177.
11. Z. V. P. Murthy and A. Choudhary, *Desalination*, 2011, **279**, 428-432.
12. P. K. Leung, C. Ponce-de-Leon, C. T. J. Low, A. A. Shah and F. C. Walsh, *J. Power Sources*, 2011, **196**, 5174-5185.
13. J. Gu, Z. Q. Zhao, Y. Ding, H. L. Chen, Y. W. Zhang and C. H. Yan, *J. Am. Chem. Soc.*, 2013, **135**, 8363-8371.
14. Z. J. Wang, J. P. Zhong, H. X. Jiang, J. Wang and H. B. Liang, *Cryst. Growth Des.*, 2014, **14**, 3767-3773.
15. A. J. Fernández-Carrión, M. Ocaña, J. García-Sevillano, E. Cantelar and A. I. Becerro, *J. Phys. Chem. C*, 2014, **118**, 18035-18043.
16. T. Uda, K. T. Jacob and M. Hirasawa, *Science*, 2000, **289**, 2326-2329.
17. C. D. Anderson, C. G. Anderson and P. R. Taylor, *Can. Metall. Q.*, 2013, **52**, 249-256.
18. M. Tanaka, T. Oki, K. Koyama, H. Narita and T. Oishi, *Handbook on the physics and chemistry of rare earths*, 2012, **43**, 159-211.
19. C. Tunsu, C. Ekberg and T. Retegan, *Hydrometallurgy*, 2014, **144**, 91-98.
20. D. Bauer, D. Diamond, J. Li, D. Sandalow, P. Telleen and B. Wanner, 2010.
21. S. Radhika, B. N. Kumar, M. L. Kantam and B. R. Reddy, *Sep. Purif. Technol.*, 2010, **75**, 295-302.
22. S. R. Dave, H. Kaur and S. K. Menon, *Reactive and Functional Polymers*, 2010, **70**, 692-698.
23. B. Kronholm, C. G. Anderson and P. R. Taylor, *Jom*, 2013, **65**, 1321-1326.

Journal of Materials Chemistry A Accepted Manuscript

24. I. Sierra and D. Perez-Quintanilla, *Chem. Soc. Rev.*, 2013, **42**, 3792-3807.
25. T. Sangvanich, V. Sukwarotwat, R. J. Wiacek, R. M. Grudzien, G. E. Fryxell, R. S. Addleman, C. Timchalk and W. Yantasee, *J. Hazard. Mater.*, 2010, **182**, 225-231.
26. V. Valtchev and L. Tosheva, *Chem. Rev. (Washington, DC, U. S.)*, 2013, **113**, 6734-6760.
27. K. C.-W. Wu and Y. Yamauchi, *J. Mater. Chem.*, 2012, **22**, 1251-1256.
28. N. Suzuki, S. Kiba and Y. Yamauchi, *J. Mater. Chem.*, 2011, **21**, 14941-14947.
29. Y.-D. Chiang, H.-Y. Lian, S.-Y. Leo, S.-G. Wang, Y. Yamauchi and K. C. W. Wu, *J. Phys. Chem. C*, 2011, **115**, 13158-13165.
30. M. Laprise-Pelletier, M. Bouchoucha, J. Lagueux, P. Chevallier, R. Lecomte, Y. Gossuin, F. Kleitz and M.-A. Fortin, *J. Mater. Chem. B*, 2015, **3**, 748-758.
31. T. Xie, L. Shi, J. Zhang and D. Zhang, *Chem. Commun.*, 2014, **50**, 7250-7253.
32. W. Y. Huang, Y. Zhu, J. P. Tang, X. Yu, X. L. Wang, D. Li and Y. M. Zhang, *J. Mater. Chem. A*, 2014, **2**, 8839-8848.
33. J. Florek, F. Chalifour, F. Bilodeau, D. Lariviere and F. Kleitz, *Adv. Funct. Mater.*, 2014, **24**, 2668-2676.
34. J. L. Vivero-Escoto, I. I. Slowing, C.-W. Wu and V. S. Y. Lin, *J. Am. Chem. Soc.*, 2009, **131**, 3462-3463.
35. D. R. Radu, C.-Y. Lai, K. Jeftinija, E. W. Rowe, S. Jeftinija and V. S. Y. Lin, *J. Am. Chem. Soc.*, 2004, **126**, 13216-13217.
36. C. E. Fowler, S. L. Burkett and S. Mann, *Chem. Commun.*, 1997, **18**, 1769-1770.
37. M. Kruk, M. Jaroniec and A. Sayari, *Langmuir*, 1997, **13**, 6267-6273.
38. G. E. Fryxell, Y. H. Lin, S. Fiskum, J. C. Birnbaum, H. Wu, K. Kemner and S. Kelly, *Environ. Sci. Technol.*, 2005, **39**, 1324-1331.
39. Z. J. Wu, H. Joo and K. Lee, *Chem. Eng. J.*, 2005, **112**, 227-236.
40. M. Mazzotti, *J. Chromatogr. A*, 2006, **1126**, 311-322.
41. S. J. Allen, G. McKay and J. F. Porter, *J. Colloid Interface Sci.*, 2004, **280**, 322-333.

Journal of Materials Chemistry A Accepted Manuscript

Figures

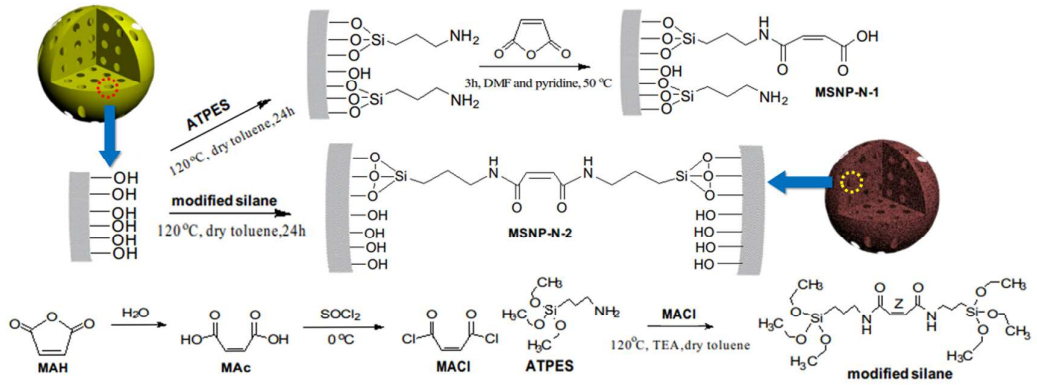

Scheme 1.

Scheme 1. Schematic illustration of the preparation of surface modified MSNPs as selective REM sorbents.

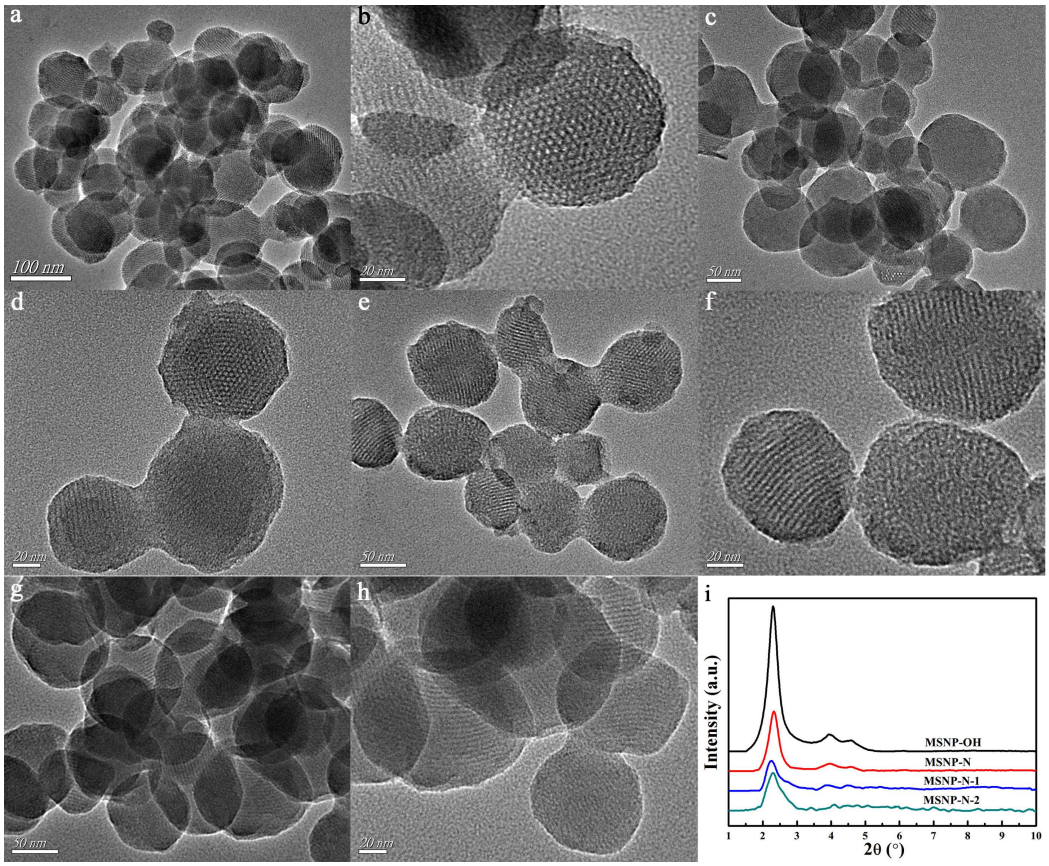

Fig. 1.

Fig. 1. Representative TEM images of MSNP-OH (a, b), MSNP-N (c, d), MSNP-N-1 (e, f), and MSNP-N-2 (g, h) under different magnifications, and low-angle XRD patterns of pristine and modified materials (i).

Journal of Materials Chemistry A Accepted Manuscript

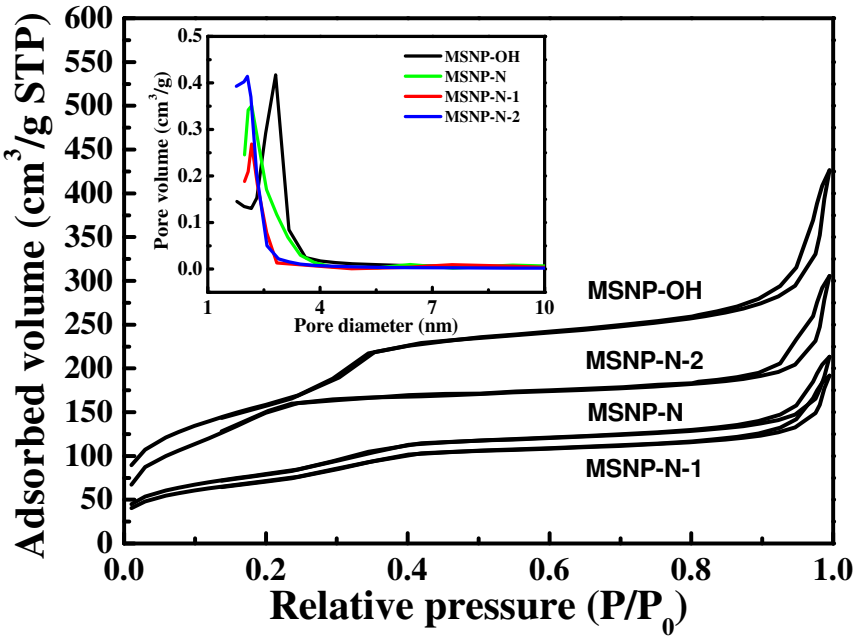

Fig. 2.

Fig. 2. N_2 adsorption-desorption isotherms and pore size distributions (insert) for MSNP-OH, MSNP-N, MSNP-N-1, and MSNP-N-2.

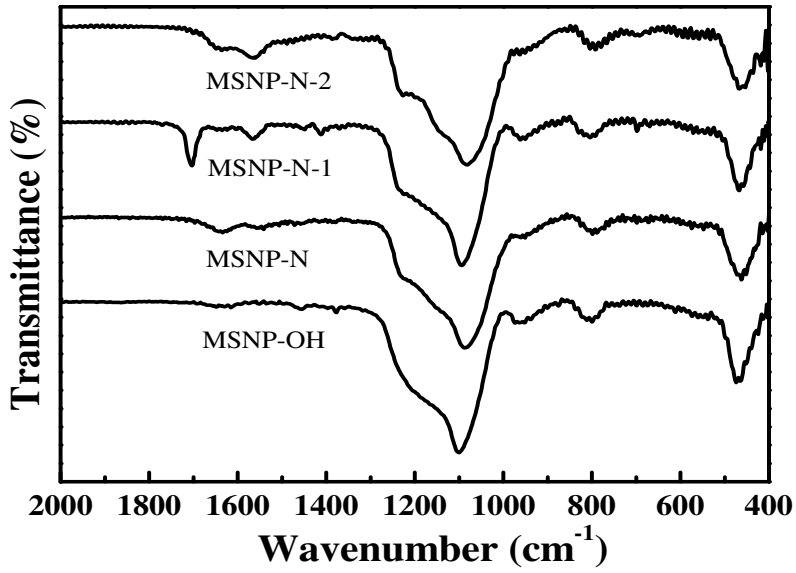

Fig. 3.

Fig. 3. FT-IR spectra for the pristine and modified materials.

Journal of Materials Chemistry A Accepted Manuscript

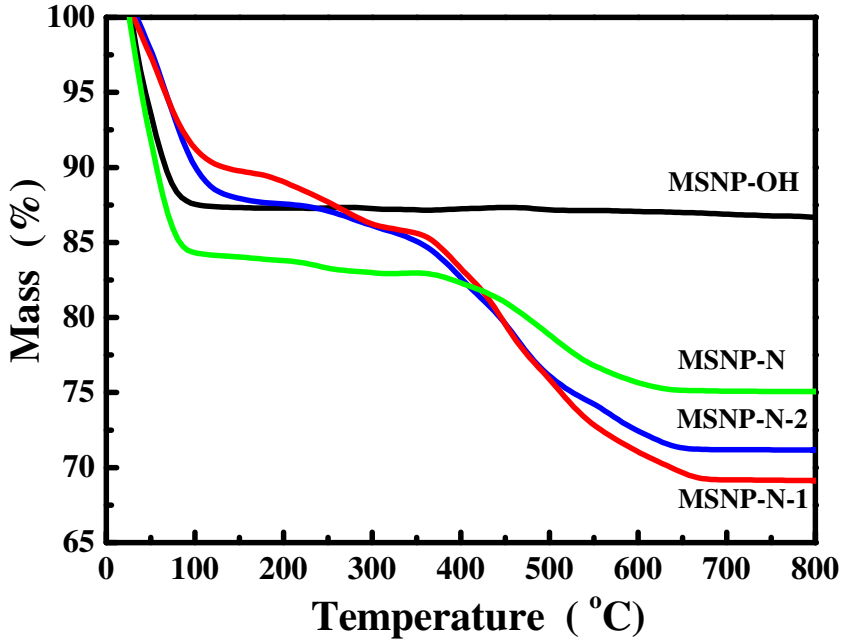

Fig. 4.

Fig. 4. Thermogravimetric analysis curves of the pristine and modified materials.

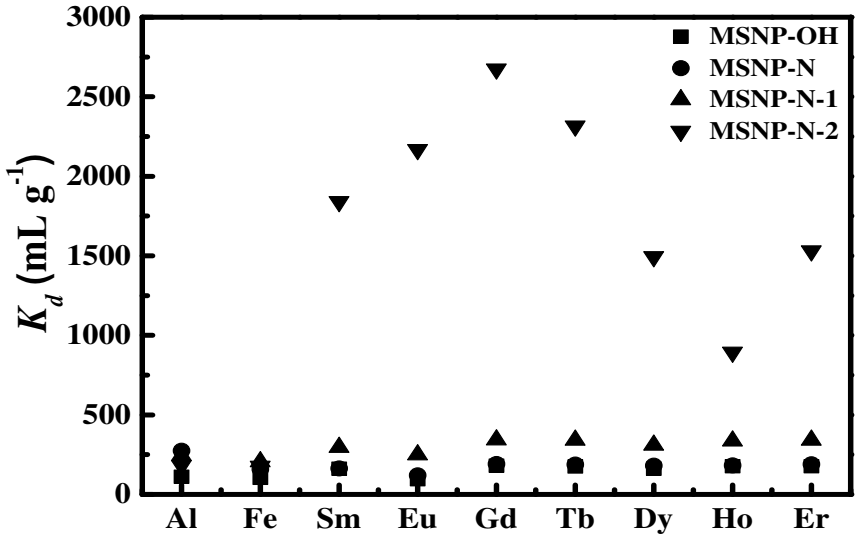

Fig. 5.

Fig. 5. K_d values of the hybrid materials for a mixture of Al, Fe, Sm, Eu, Gd, Tb, Dy, Ho, and Er. The standard deviation of the analyses can be seen in Fig. S2.

Journal of Materials Chemistry A Accepted Manuscript

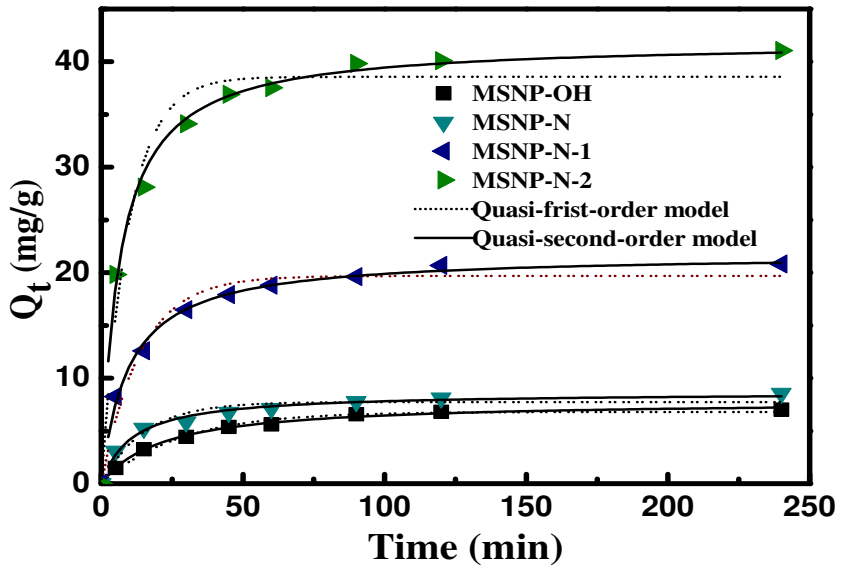

Fig. 6.

Fig. 6. Kinetic data and modelling for the adsorption of Gd^{3+} on MSNP-OH, MSNP-N, MSNP-N-1, and MSNP-N-2. The standard deviation of the kinetic data can be seen in Fig. S3.

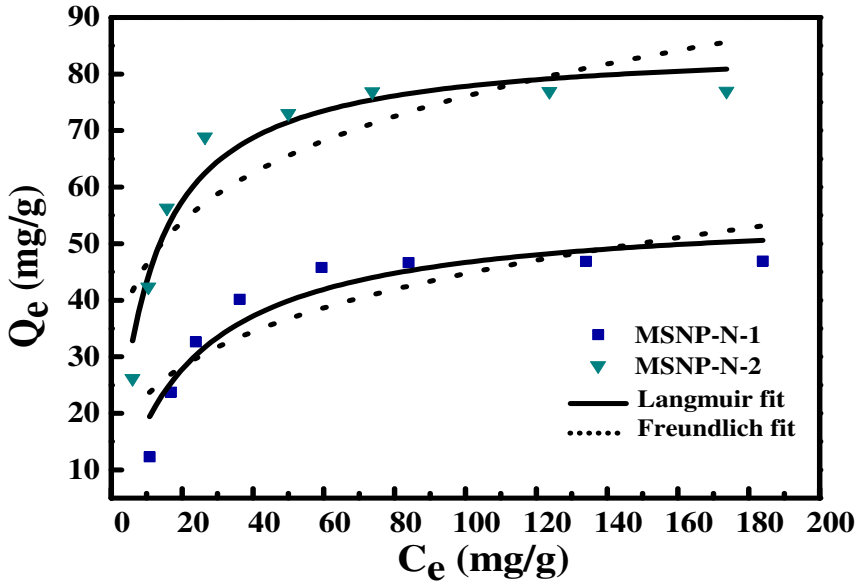

Fig. 7.

Fig. 7. Equilibrium data and modelling for the adsorption of Gd^{3+} on MSNP-OH, MSNP-N, MSNP-N-1, and MSNP-N-2. The standard deviation of isotherm data can be seen in Fig. S4.

Journal of Materials Chemistry A Accepted Manuscript

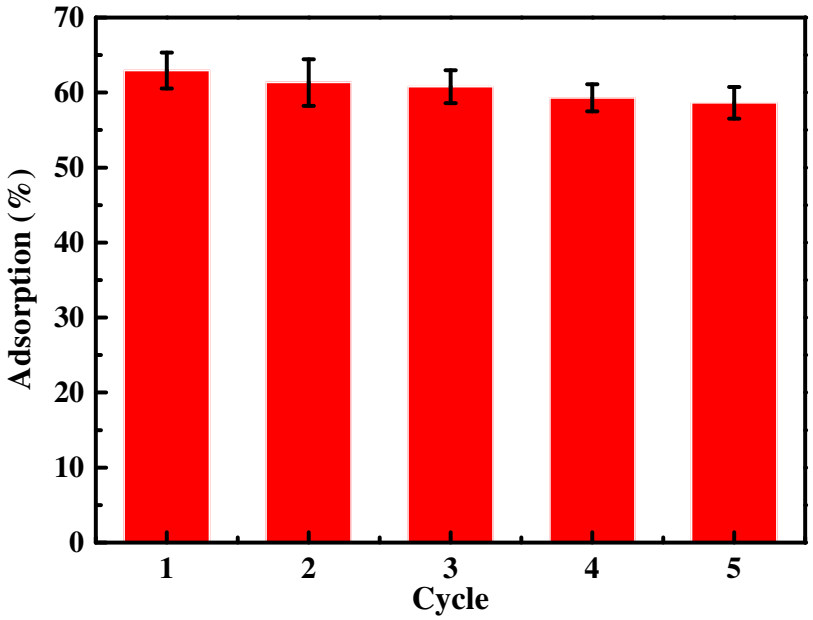

Fig. 8.

Fig. 8. Regeneration of MSNP-N-2 over 5 cycles. Error bars represent the standard error of the mean for measurements carried out in triplicate.

Journal of Materials Chemistry A Accepted Manuscript

Table 1: Elemental Composition of the materials from Elemental Analysis

1	N (%)	C (%)	H(%)	[Cl-] (mol g^{-1})
MSNP-OH	-	-	2.709	-
MSNP-N	4.962	14.39	3.835	-
MSNP-N-1	5.416	15.70	3.851	-
MSNP-N-2	5.209	18.16	3.902	0.00015 (RSD=4.546%)

Table 2: Kinetic constants for the Pseudo-first-order and Pseudo-second-order models

Materials	$Q_{e,exp}$ (mg g^{-1})	Pseudo-first-order kinetic model			Pseudo-second-order kinetic model				
		$Q_{e,c}$ (mg g^{-1})	k_1 (L min^{-1})	R^2	$Q_{e,c}$ (mg g^{-1})	$k_2\times10^{-2}$(g $mg^{-1}min^{-1}$	h (mg $g^{-1}min^{-1}$	$t_{1/2}$ (min)	R^2
MSNP-OH	7.418	6.803	0.0366	0.988	7.862	0.801	0.494	21.60	0.993
MSNP-N	8.375	7.742	0.0663	0.943	8.657	1.066	0.798	10.83	0.967
MSNP-N-1	20.82	19.69	0.0726	0.971	21.78	0.483	2.291	9.507	0.987
MSNP-N-2	41.06	38.56	0.1050	0.961	41.94	0.376	6.614	5.367	0.985

Table 3 Adsorption equilibrium constants for Langmuir and Freundlich isotherm equations

Sorbents	Langmuir isotherm equation				Freundlich isotherm equation		
	R^2	K_L (L mg^{-1})	Q_m (mg g^{-1})	R_L	R^2	K_F (mg g^{-1})	$1/n$
MSNP-N-1	0.889	0.0488	56.22	0.0929	0.698	12.04	0.2846
MSNP-N-2	0.942	0.1031	85.38	0.0463	0.727	28.31	0.2147

Journal of Materials Chemistry A Accepted Manuscript